

Pixelated phase computer holograms for the accurate encoding of scalar complex fields

Victor Arrizón,^{1,*} Ulises Ruiz,¹ Rosibel Carrada,¹ and Luis A. González²

¹*Instituto Nacional de Astrofísica, Óptica y Electrónica, Apdo. Postal 51 y 216, Puebla PUE 72000, México*

²*Departamento de Investigación en Física, Universidad de Sonora, Apdo. Postal 5-88, Hermosillo SON 83190, México*

*Corresponding author: arrizon@inaoep.mx

Received April 24, 2007; revised August 27, 2007; accepted August 28, 2007;
posted August 30, 2007 (Doc. ID 82363); published October 16, 2007

We discuss a class of phase computer-generated holograms for the encoding of arbitrary scalar complex fields. We describe two holograms of this class that allow high quality reconstruction of the encoded field, even if they are implemented with a low-resolution pixelated phase modulator. In addition, we show that one of these holograms can be appropriately implemented with a phase modulator limited by a reduced phase depth. © 2007 Optical Society of America

OCIS codes: 090.1760, 090.2890, 100.5090, 090.1970, 230.6120, 070.0070.

1. INTRODUCTION

The generation of complex scalar optical fields with amplitude and phase spatial modulations that are independently specified is an important task in contemporary optics. A practical and versatile method for generating these arbitrary complex fields is based on the use of computer-generated holograms (CGHs) [1–12]. In particular, the use of phase CGHs is especially convenient because of their relatively high efficiency [6–11]. It is important to distinguish cell-oriented and point-oriented holograms for encoding complex fields. In general, point-oriented approaches [6,9–12] are more convenient when holograms are implemented with low-resolution pixelated modulators.

When a pixelated spatial light modulator (SLM) is employed to implement a CGH, the quality of the reconstructed field can be seriously affected by noise originating in high-order diffraction field contributions. Here we discuss a class of phase CGHs that encode arbitrary scalar complex fields. We show that two of the CGHs that belong to this class provide appropriate reconstruction of the encoded fields, even if they are implemented with a low-resolution pixelated phase SLM. The good performance of these CGHs is enabled by a significant reduction in the relative intensity of the high-order diffraction field contributions that share the spatial frequency domain of the encoded field. One of the proposed holograms can be implemented with a phase SLM that provides a reduced phase range (close to π rad). We report the experimental implementation of this last hologram by means of a translucent, twisted, nematic liquid-crystal (LC) SLM.

The content is organized as follows. In Section 2 we present the theory of our proposal. In Section 3 we evaluate and compare the performance of the discussed holograms when a pixelated SLM is employed for their implementation. In Section 4 we report the experimental

realization of one of the discussed holograms, and in Section 5 we present remarks and conclusions.

2. THEORETICAL FORMULATION

Our purpose is to generate an arbitrary complex optical field whose amplitude and phase modulations are independently specified. This complex field can be expressed as

$$s(x,y) = a(x,y)\exp[i\phi(x,y)], \quad (1)$$

where the amplitude $a(x,y)$ and the phase $\phi(x,y)$ take values in the intervals $[0, 1]$ and $[-\pi, \pi]$, respectively. The complex amplitude values of the function $s(x,y)$ belong to the set of complex numbers with modulus equal to or smaller than one, which is denoted as Ω_S . Our aim is to encode the complex field $s(x,y)$ by means of a phase transmittance CGH. In general, a CGH that encodes the arbitrary complex modulation $s(x,y)$ has a constrained complex transmittance with values in a subset of Ω_S . In the case of phase CGHs, this subset is formed by the complex points of unity modulus. The transmittance of a phase CGH, expressed as a function explicitly dependent on the amplitude and the phase of the encoded field, is given by

$$h(x,y) = \exp[i\psi(a, \phi)], \quad (2)$$

where $\psi(a, \phi)$ is the CGH phase modulation.

The explicit dependence of the amplitude a and the phase ϕ on the spatial coordinates (x,y) has been omitted in Eq. (2). Our purpose is to establish phase functions with the form of Eq. (2) that provide the appropriate encoding of the complex field $s(x,y)$. A fruitful method to determine appropriate forms of the hologram phase modulation $\psi(a, \phi)$ is based on the representation of $h(x,y)$ by a Fourier series in the domain of ϕ . Developing this Fourier series, the CGH transmittance can be expressed as

$$h(x,y) = \sum_{q=-\infty}^{\infty} h_q(x,y), \quad (3)$$

where

$$h_q(x,y) = c_q^a \exp(iq\phi), \quad (4)$$

$$c_q^a = (2\pi)^{-1} \int_{-\pi}^{\pi} \exp[i\psi(\phi,a)] \exp(-iq\phi) d\phi. \quad (5)$$

In Eq. (5) it is noted that after integration in the variable ϕ , the resulting coefficients c_q^a remain explicitly dependent on the amplitude a . Therefore, the coefficients c_q^a are implicitly dependent on the coordinates (x,y) . The signal $s(x,y)$ is recovered from the first-order term $h_1(x,y)$ in the series of Eq. (3) if the identity

$$c_1^a = Aa \quad (6)$$

is fulfilled for a positive constant A . This identity is referred to as the signal encoding condition.

Sufficient and necessary conditions to fulfill Eq. (6) are given by the following equations:

$$\int_{-\pi}^{\pi} \sin[\psi(\phi,a) - \phi] d\phi = 0, \quad (7)$$

$$\int_{-\pi}^{\pi} \cos[\psi(\phi,a) - \phi] d\phi = 2\pi Aa. \quad (8)$$

Equations (7) and (8) provide a useful basis for determination of appropriate CGHs. The phase functions $\psi(\phi,a)$ that obey these equations define a specific class of phase CGHs. It is noted that the maximum of the integral in Eq. (8) is 2π . Thus, the maximum possible value of the constant A in the encoding condition [Eq. (6)] is one. This result provides a limit to the efficiency of the CGHs that belong to this class. In the remaining discussion we focus our attention on functions $\psi(\phi,a)$ with odd symmetry in the variable ϕ . The symmetry of such functions ensures the fulfillment of Eq. (7).

A. Phase CGH of Type 1

As first example we consider a CGH that is essentially equivalent to a synthetic hologram already found in optics literature [9]. The phase modulation of this hologram can be expressed as

$$\psi(\phi,a) = f(a)\phi, \quad (9)$$

where the factor $f(a)$ remains undetermined for the moment. The q th-order Fourier series coefficient for this CGH computed with Eq. (5) is

$$c_q^a = \text{sinc}[q - f(a)], \quad (10)$$

where $\text{sinc}(\xi) \equiv (\pi\xi)^{-1} \sin(\pi\xi)$. If $f(a)$ is obtained from the relation

$$\text{sinc}[1 - f(a)] = a, \quad (11)$$

then the encoding condition [Eq. (6)] is fulfilled with $A = 1$. For the complete definition of the CGH, the function $f(a)$ is numerically inverted from Eq. (11). The computed

values of $f(a)$ versus a are shown in Fig. 1 (solid curve).

Next we analyze two additional phase functions $\psi(\phi,a)$ that, to the best of our knowledge, correspond to phase CGHs that are reported here for the first time.

B. CGH of Type 2

Another phase modulation $\psi(\phi,a)$, with odd symmetry in ϕ , is given by

$$\psi(\phi,a) = \phi + f(a)\sin(\phi). \quad (12)$$

The phase CGH transmittance in this case is $h(x,y) = \exp(i\phi)\exp[if(a)\sin(\phi)]$. The Fourier series in the variable ϕ for this phase transmittance can be directly found by using the Jacobi–Anger identity [13]. According to this identity, the second phase factor in the CGH transmittance $h(x,y)$ is given by

$$\exp[if(a)\sin(\phi)] = \sum_{m=-\infty}^{\infty} J_m[f(a)] \exp(im\phi), \quad (13)$$

where J_m denotes an integer-order Bessel function. Considering this relationship it is readily proved that the new CGH transmittance $h(x,y)$ is expressed by the Fourier series defined in Eqs. (3) and (4) with coefficients

$$c_q^a = J_{q-1}[f(a)]. \quad (14)$$

According to Eq. (14), the encoding condition [Eq. (6)] is valid (with $A = 1$) if $f(a)$ is obtained from the relation

$$J_0[f(a)] = a. \quad (15)$$

Equation (15) can be fulfilled for every value of a in the interval $[0,1]$ by taking the appropriate value of $f(a)$ in the domain $[0,x_0]$, where $x_0 \cong 2.4048$ is the first positive root of the Bessel function $J_0(x)$. The resulting function $f(a)$, numerically generated from Eq. (15), is plotted in Fig. 1 (dashed curve).

C. CGH of Type 3

The second new CGH that we propose is associated with the phase modulation

$$\psi(\phi,a) = f(a)\sin(\phi). \quad (16)$$

Although this CGH phase function is similar to the function in Eq. (12), it presents special features that justify its discussion. To obtain the Fourier series and corresponding coefficients for this CGH we employ again the Jacobi–

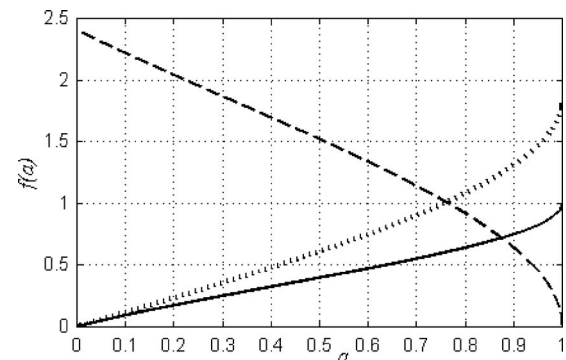


Fig. 1. Function $f(a)$ versus a for the CGHs of types 1 (solid curve), 2 (dashed curve), and 3 (dotted curve).

Anger identity [Eq. (13)]. The resulting q th-order coefficient in this Fourier series is

$$c_q^a = J_q[f(a)], \quad (17)$$

and the encoding condition is fulfilled if $f(a)$ is inverted from the relation

$$J_1[f(a)] = Aa. \quad (18)$$

The maximum value of A for which Eq. (18) can be fulfilled is $A \cong 0.5819$, which corresponds to the maximum value of the first-order Bessel function $J_1(x)$, which occurs in turn at $x = x_1 \cong 1.84$.

The function $f(a)$ obtained by numerical inversion from Eq. (18) adopts values in the interval $[0, x_1]$ [see Fig. 1 (dotted curve)]. It is interesting to note, considering the limit values of $f(a)$ and Eq. (16), that this CGH can be implemented with phase modulation in a reduced domain $[-f_0\pi, f_0\pi]$ with $f_0 \cong 0.586$. The phase range of the required modulator in this case is $\Delta\phi = 2f_0\pi \cong 1.17\pi$.

A further reduction in this phase range can be attained by adopting a smaller value of A in Eq. (18). An advantage of this reduced phase domain is that it can be easily obtained with conventional LC SLMs employing relatively long wavelengths, e.g., in the near-infrared domain. This type of illumination is appropriate for manipulation of living cells with optical tweezers [14–16]. It will be shown in Section 3, that in spite of the phase range reduction in the CGH defined by Eq. (16), it allows the accurate encoding of complex fields.

D. Modification of the Hologram by a Phase Carrier

We assume that the reconstruction of the encoded field is performed by spatial filtering in the hologram Fourier spectrum plane. The optical setup for reconstruction is schematically represented in Fig. 2. It is assumed that the CGH is placed at the back focal plane of the first lens (L1). The Fourier transform of the field transmitted by the CGH is formed at the spatial filter plane. In general, the CGH spectrum is formed by the signal term and non-signal or high-order spectrum field contributions. For reconstruction of the encoded field with high signal-to-noise ratio (SNR) a minimal overlapping is desired between the signal and the high-order terms in the CGH spectrum. Under this condition, a spatial filter pupil can be employed to transmit the light corresponding to the Fourier spectrum of the encoded field. The encoded field itself is

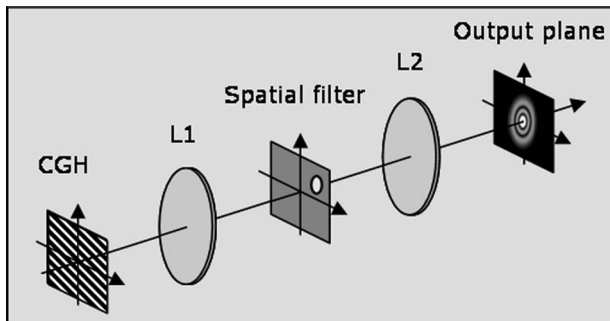


Fig. 2. Double-Fourier transform optical setup for the generation of scalar complex fields employing a CGH.

generated by the second Fourier transforming lens (L2) at the output plane of the setup.

Next we discuss a modification of the CGH defined in Eq. (2) that enables the isolation of signal from noise in the CGH Fourier spectrum domain. The Fourier spectrum of the encoded field $s(x, y)$ is denoted by $S(u, v)$, where (u, v) represent the spatial frequency coordinates associated with the spatial coordinates (x, y) . If we assume that the Fourier spectrum $S(u, v)$ is centered on the Fourier plane axis $(u, v) = (0, 0)$, then the spectra for the different terms $h_q(x, y)$ in the hologram Fourier expansion [Eq. (3)] are also centered on this axis. Thus, the encoded field can not be recovered by spatial filtering from the CGH defined in Eq. (2).

To achieve the spatial isolation of the encoded field, the above definition of the CGH is modified by adding the carrier phase modulation $2\pi(u_0x + v_0y)$ with spatial frequencies (u_0, v_0) to the phase of the encoded field. The modified CGH transmittance $h_c(x, y) = \exp[i\psi(\phi + 2\pi(u_0x + v_0y), a)]$ can be expressed by the Fourier series

$$h_c(x, y) = \sum_{q=-\infty}^{\infty} h_q(x, y) \exp[i2\pi(qu_0x + qv_0y)]. \quad (19)$$

The Fourier spectrum of this modified CGH is given by

$$H_c(u, v) = \sum_{q=-\infty}^{\infty} H_q(u - qu_0, v - qv_0), \quad (20)$$

where $H_q(u, v)$ is the Fourier transform of $h_q(x, y)$ [defined by Eq. (4)]. The structure of the CGH Fourier transform formed by laterally shifted copies of the Fourier spectra $H_q(u, v)$ allows the spatial isolation of the encoded field, whose Fourier spectrum appears as $H_1(u - u_0, v - v_0)$. The distribution of the CGH spectra terms $H_q(u - qu_0, v - qv_0)$ when $u_0 = v_0$ is schematically represented in Fig. 3. The zeroth-order $H_0(u, v)$ appears at the center of this figure.

The Fourier spectrum in Eq. (20) corresponds to a CGH implemented with a phase modulator free of spatial quantization. Accurate implementation of CGHs without spatial quantization allows an efficient isolation of the en-

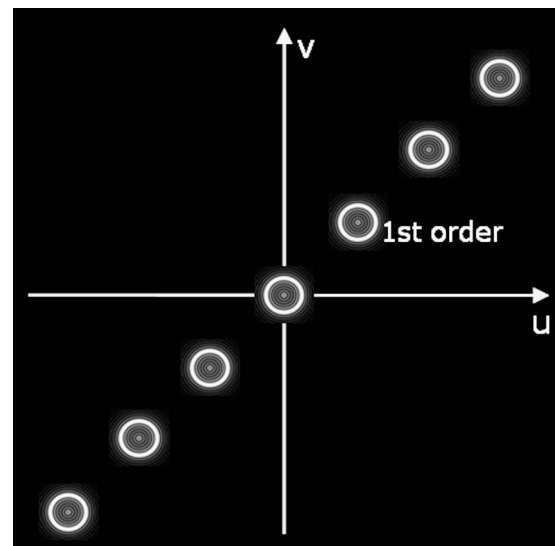


Fig. 3. Schematic spatial distribution of the CGH spectra terms $H_q(u - qu_0, v - qv_0)$ when $u_0 = v_0$.

coded field from nonsignal diffraction orders of the CGH, enabling reconstruction with a high SNR. A requirement (common to all the CGH types) for obtaining an acceptable SNR is that at least one of the hologram carrier frequencies (u_0, v_0) be larger than the bandwidth of the encoded field $s(x, y)$. On the other hand, if a CGH is implemented with a low-resolution pixelated SLM, the reconstructed signal term can be significantly affected by high-order diffraction contributions. In general, the noise level in the reconstructed field introduced by the high-order diffraction terms is highly dependent on the CGH type. In Section 3 we prove that the two new proposed CGHs (of types 2 and 3) can generate the encoded complex field with high SNR even if they are implemented with a pixelated SLM.

An alternate method of attempting the separation of signal from noise is based on the addition of a quadratic phase carrier (see, e.g., [17]) to the phase of the encoded field. If the resulting CGH is illuminated by a plane wave, the Fourier transforms of the different terms $h_q(x, y)$ of the CGH Fourier series are generated at different planes in the Fresnel domain of the CGH. A drawback of this method is that part of the high-order noise field contributions appear in a diluted form at the plane where the Fourier transform of the encoded signal is obtained.

3. IMPLEMENTATION OF PHASE HOLOGRAMS WITH A PIXELATED SLM

Let us assume that the CGHs are implemented with a pixelated phase SLM. For simplicity we assume that the SLM pixel pitch δx is the same in the horizontal and the vertical axes and that the pixels are squares of side b . Thus, the Fourier spectrum of the pixelated CGH is given by

$$H_{pix}(u, v) = E(u, v) \sum_{n=-\infty}^{\infty} \sum_{m=-\infty}^{\infty} H_c(u - n\Delta u, v - m\Delta v), \quad (21)$$

where $\Delta u = 1/\delta x$ is the SLM bandwidth, $E(u, v) = b^2 \text{sinc}(bu) \text{sinc}(bv)$ is the Fourier transform of the square pixel, and $H_c(u, v)$ is the Fourier spectrum of the continuous CGH given by Eq. (20). According to Eq. (21), the Fourier spectrum of the pixelated CGH is formed by the superposition of laterally shifted replicas of the spectrum $H_c(u, v)$ modulated by the pixel Fourier transform $E(u, v)$. The spectrum function $H_1(u - u_0, v - v_0)$ that appears at the term $H_c(u, v)$ of the series in Eq. (21) is equivalent to the signal spectrum $S(u - u_0, v - v_0)$. The distortion of the signal spectrum due to the factor $E(u, v)$ can be avoided by an appropriate prefiltering of the encoded field [12]. This process consists in replacing the original encoded field $s(x, y)$ by a modified field $s'(x, y)$ that is defined by its Fourier transform $S'(u, v)$ obtained from the relation $S'(u - u_0, v - v_0) = S(u - u_0, v - v_0)E^{-1}(u, v)$. The function $E^{-1}(u, v)$ is appropriately defined in the domain of $S(u - u_0, v - v_0)$ since the carrier frequencies (u_0, v_0) are always chosen in such a way that $S(u - u_0, v - v_0)$ is enveloped by a nonzero sector of $E(u, v)$. This prefiltering is applied to the complex fields that are holographically en-

coded below either by numerical simulations or experimentally.

An inconvenient consequence of the pixelated structure of the CGH is that the domain of the signal spectrum term $H_1(u - u_0, v - v_0)$ that is centered at the spatial frequency coordinates (u_0, v_0) may also contain high-order spectrum contributions H_q that are members of several of the spectrum replicas $H_c(u - n\Delta u, v - m\Delta v)$. To analyze the relative significance of the high-order spectrum terms H_q sharing the signal spectrum region, let us assume that the carrier spatial frequencies are $u_0 = v_0 = (P/Q)\Delta u$ with relative prime integers P and Q . In this case, it is not difficult to prove that the spectra contributions that appear centered at the signal spatial frequencies (u_0, v_0) are $H_{QR+1}(u - u_0, v - v_0)$ for any arbitrary integer number R . The signal term in this set of spectra contributions corresponds to $R = 0$.

To prove this result, we first note that for the assumed carrier frequencies $u_0 = v_0 = (P/Q)\Delta u$, the spectra terms H_q in Eq. (20) take the form $H_q(u - qu_0, v - qu_0)$. This means that all the terms H_q in $H_c(u, v)$ are centered at the axis $u = v$ in the CGH Fourier spectrum domain. As a particular case, the signal spectrum term $H_1(u - u_0, v - v_0)$ is also centered at the coordinates (u_0, v_0) . Another important observation is that the only terms $H_c(u - n\Delta u, v - m\Delta v)$ in Eq. (21) that contain spectra functions H_q placed at the axis $u = v$ are those with indices $n = m$. Considering the relation $u_0 = v_0 = (P/Q)\Delta u$, the term $H_c(u - n\Delta u, v - n\Delta v)$ can be expressed as

$$H_c(u - n\Delta u, v - n\Delta v) = \sum_{q=-\infty}^{\infty} H_q[u - (nQ/P + q)u_0, v - (nQ/P + q)v_0]. \quad (22)$$

It can be directly verified that the functions H_q in Eq. (22) that appear centered at coordinates (u_0, v_0) are those corresponding to the combination of indices $n = -RP$ and $q = QR + 1$ for any integer R . This proves that the Fourier spectrum of the pixelated CGH contains the terms $H_{QR+1}(u - u_0, v - v_0)$ for any integer R that are centered at the coordinates (u_0, v_0) . It must be emphasized that in this collection of spectra terms the spectrum of the encoded field corresponds to $R = 0$.

To obtain a high SNR, the high-order contributions $H_{QR+1}(u - u_0, v - v_0)$ (with $R \neq 0$) must be negligible compared with the signal spectrum $H_1(u - u_0, v - v_0)$. Considering Eq. (4), it is clear that the power of the spectrum term $H_{QR+1}(u, v)$ is proportional to the squared modulus of the coefficient c_{QR+1}^a . It is interesting to note that coefficients c_q^a for the CGHs of types 2 and 3 defined in Eqs. (14) and (17) in terms of Bessel functions tend rapidly to zero when $|q|$ is increased. Thus, it is expected that (for a moderately large Q) these CGHs will enable reconstruction of the encoded field with relatively high SNR.

The significance of noise contribution $H_{QR+1}(u - u_0, v - v_0)$ in relation to the signal term $H_1(u - u_0, v - v_0)$ can be measured by the ratio $\rho = |c_{QR+1}^a|^2 / |c_1^a|^2$. As an example let us assume $P = 1$ and $Q = 6$ (i.e., $u_0 = v_0 = \Delta u/6$). In this case, the dependence of $\log(\rho)$ (for $R = 1$ and 2) on the amplitude a for the different CGH types is shown in Fig. 4. The lower values of $\log(\rho)$ for the CGH of types 2 and 3 are evident.

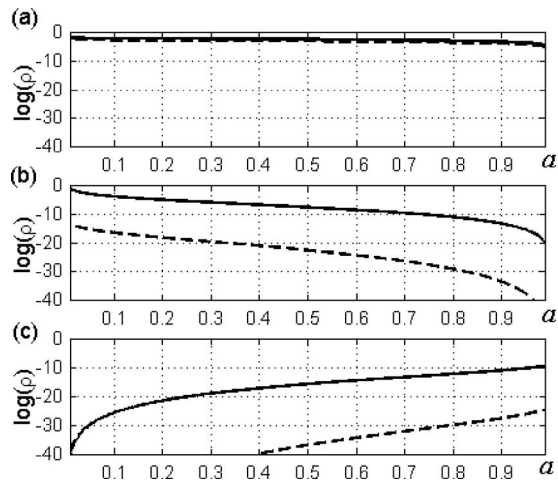


Fig. 4. Function $\log(\rho)$ versus α , where $\rho = |c_{QR+1}^a|^2 / |c_1^a|^2$ (for $Q = 6$) for the CGHs of types (a) 1, (b) 2, and (c) 3. The values of index R are 1 (solid curve) and 2 (dashed curve).

The parameter $\rho = |c_{QR+1}^a|^2 / |c_1^a|^2$ is useful to evaluate the quality of CGHs without requiring knowledge of the encoded complex function $s(x, y)$. Lower values of ρ correspond to CGHs with higher immunity to the high-order noise terms that are transmitted in the CGH plane. The SNR provides another measure of the CGH performance. Contrasting with the parameter ρ , the SNR, which is employed below for evaluation of different CGHs, is explicitly dependent on the form of the encoded field $s(x, y)$. It must be emphasized that low-order nonsignal spectrum field contributions (of order $q \neq QR + 1$) also present replicas due to the SLM sampling. However none of these spectrum replicas appears centered on the signal frequencies (u_0, u_0) . On the other hand, the low-order nonsignal spectrum field contributions (e.g., of orders 0 or 2) can partially overlap the signal spectrum. However, this influence can be minimized either by increasing the carrier frequencies (u_0, u_0) or by reducing the bandwidth of the encoded signal. This control is possible because in general a reduction of the encoded signal bandwidth also reduces the bandwidth of the high-order CGH terms.

To illustrate the performance of pixelated CGHs we employ these holograms to encode Laguerre–Gauss beams. These beams are expressed in polar coordinates (r, θ) as

$$u(r, \theta) = C(\sqrt{2}r/w_0)^{|l|} L_p^{|l|}(2r^2/w_0^2) \exp(-r^2/w_0^2) \exp(il\theta). \tag{23}$$

In Eq. (23) $L_p^{|l|}$ denotes an associated Laguerre polynomial, w_0 is the beam waist radius, p is the radial mode index, l is the phase singularity charge, and C is a normalization constant. For the first numerical simulation the waist radius is $w_0 = 40\delta x$ (recall that δx is the SLM pixel pitch), the beam indices are $(p, l) = (1, 1)$, and the beam support is a circle of radius $R = 128\delta x$. The phase tilt added to the phase of the encoded field has spatial frequencies $u_0 = v_0 = \Delta u / 6$. We designed the CGHs of types 1, 2, and 3 to encode the Laguerre–Gauss beam with such parameters.

The phase distributions for the designed CGHs of types 2 and 3 are displayed in Fig. 5. On the other hand, Fig. 6 shows the spectrum modulus of the encoded beam defined

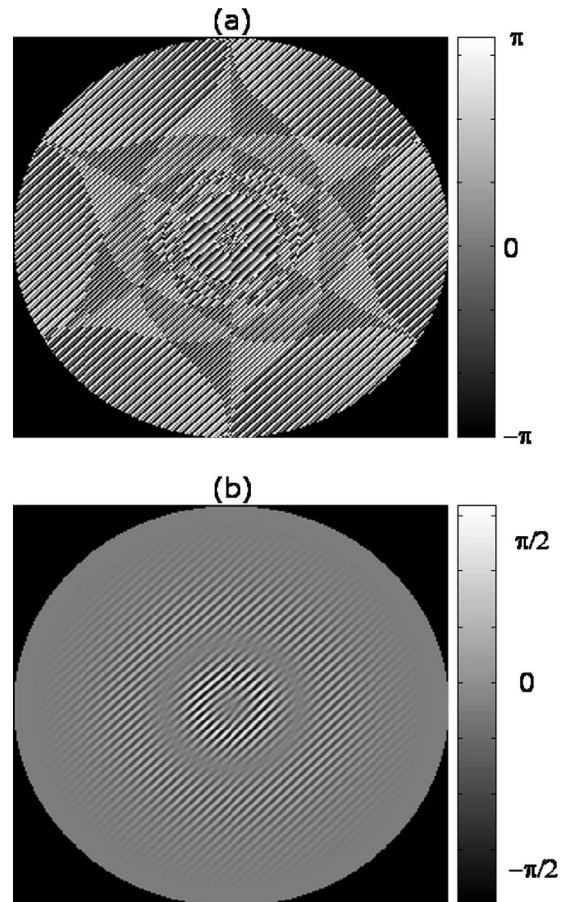


Fig. 5. Phase distributions of CGHs of (a) type 2 and (b) type 3 that encode a Laguerre–Gauss beam of indices $(p, l) = (1, 1)$.

by Eq. (23) and the moduli of the signal spectra obtained with the pixelated CGHs. It is noted that the signal spectra for the CGHs of types 2 and 3 [Fig. 6(b) and 6(c)] are quite similar to the spectrum of the encoded beam [Fig.

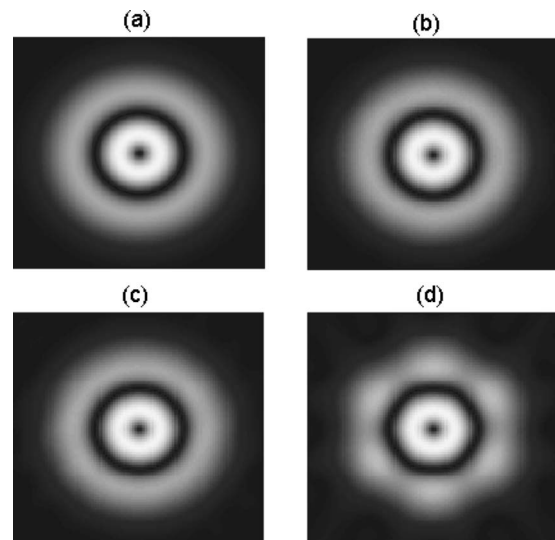


Fig. 6. (a) Spectrum modulus of a complex Laguerre–Gauss beam with indices $(p, l) = (1, 1)$, and signal spectrum modules obtained with CGHs of types (b) 2, (c) 3, and (d) 1 that encode this beam.

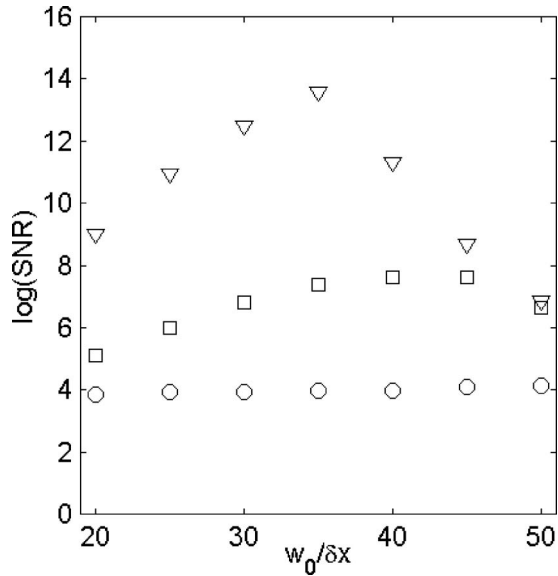


Fig. 7. Function $\log(\text{SNR})$ versus the normalized waist $w_0/\delta x$ for CGHs of types 1 (circles), 2 (squares), and 3 (triangles) designed to encode a Laguerre–Gauss beam of indices $(p, l) = (2, 2)$.

6(a)]. On the other hand, the modulus of the signal spectrum for the CGH of type 1 displayed in Fig. 6(d) shows significant distortions.

We computed the SNR of the reconstructed beams employing a conventional definition of this parameter [12] and obtaining the values of 50, 3.5×10^3 , and 3.6×10^5 for the CGHs of types 1, 2, and 3, respectively. This SNR is given by the power of the encoded field $s(x, y)$ normalized by the power of the error in the reconstructed signal. This error is expressed as $s(x, y) - \beta s_r(x, y)$, where $s_r(x, y)$ is the reconstructed signal that includes noise distortions due to high-order diffraction terms, and β is a constant that is determined to minimize the error power.

Starting with the parameters of the CGHs employed in the first simulation, we performed other numerical simulations changing the indices (p, l) , the spatial frequency of the encoded beam, and the carrier spatial frequencies (u_0, v_0) , finding that the higher SNR values are provided by the CGHs of types 2 and 3. An example of these additional results in Fig. 7 displays the logarithm of the SNR provided by CGHs designed to encode a Laguerre–Gauss beam of indices $(p, l) = (2, 2)$ with variable ratio $w_0/\delta x$. The superior SNR provided by CGHs of types 2 and 3 was also verified (by numerical simulations) for the encoding of different complex beams as the high-order nondiffracting Bessel beams.

4. EXPERIMENTAL GENERATION OF COMPLEX BEAMS WITH TYPE 3 CGH

We implemented experimentally CGHs for the synthesis of nondiffracting Bessel beams and Laguerre–Gauss beams employing a twisted nematic LC device (the LC2002 SLM of HoloEye Photonics AG). We configured this device as a phase-mostly modulator employing a linear polarizer followed by a quarter-wave plate at the input and a second linear polarizer at the output [18,19]. To minimize modulation errors produced by the nonuniform

spatial response in the SLM we employed a zone of 200×200 pixels in this device. The voltage applied to the SLM pixels are related to the gray levels of images supplied to the SLM by a PC video card. The phase modulation (versus the gray level) provided by the SLM illuminated with a He–Ne laser (633 nm) is depicted in Fig. 8(a). This phase modulation appears coupled with the amplitude modulation plotted in Fig. 8(b). Considering the reduced phase modulation range of the SLM, we employed it to display CGHs of type 3. For the design of these CGHs we neglected the coupled amplitude modulation.

The encoded Laguerre–Gauss beams are analytically expressed by Eq. (23) and the Bessel beams are represented in polar coordinates as $J_n(2\pi r/r_0)\exp(in\theta)$, where r_0 is the asymptotic radial period. For all the encoded beams we employed a finite circular support with a radius R equal to 100 pixels (of the SLM). Both the radial period r_0 (for Bessel beams) and the waist radius w_0 (for Laguerre–Gauss beams) were adopted as $R/4$. For isolation of the signal from high-order diffraction terms, we employed the carrier spatial frequencies $u_0 = v_0 = \Delta u/5$. A circular pupil in the Fourier domain of the CGHs employed as spatial filter for signal isolation was adjusted to optimize the quality of the generated fields. Because of the symmetry of the encoded fields, the pupil employed as a spatial filter in the experiment was circular. The application of this pupil to the signal spectrum represents a low-pass filtering during reconstruction of the encoded field. To increase the fidelity of the reconstructed field it is necessary to increase the pupil diameter. However, if the diameter is too large, higher amounts of noise contribution will be transmitted by the pupil. Thus, in practice it is necessary to optimize this diameter for each particular CGH. The intensity distributions of the experimentally generated beams were recorded with a CCD camera. Intensities of the generated Bessel beams of orders $n = 1, 2,$

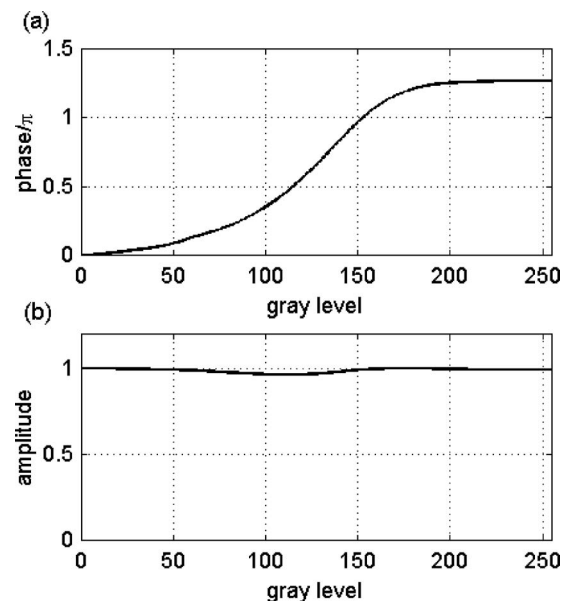


Fig. 8. (a) Phase and (b) amplitude modulations provided by a translucent twisted nematic LC device (LC2002 of HoloEye Photonics LG) configured as a phase-mostly modulator.

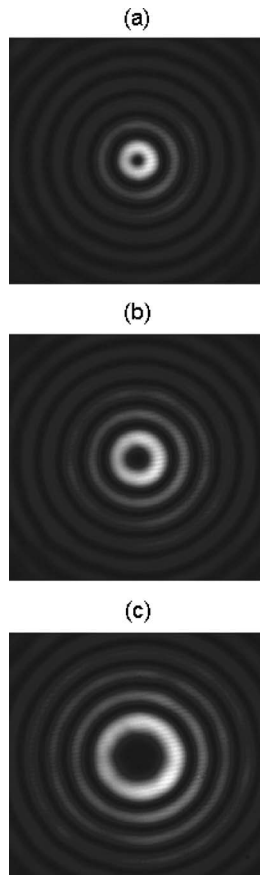


Fig. 9. Experimentally recorded intensity distributions of non-diffracting Bessel beams of orders (a) 1, (b) 2, and (c) 4 generated by type 3 CGHs employing the SLM modulation displayed in Fig. 8.

and 4 are shown in Fig. 9. The images of the generated Laguerre–Gauss beams with indices (p, l) of $(0, 2)$, $(0, 4)$, and $(2, 4)$ appear in Fig. 10.

5. FINAL REMARKS AND CONCLUSIONS

We have discussed a class of phase CGHs for encoding arbitrary scalar complex fields. We have specified the conditions that a CGH of this class must fulfill to encode the complex field and discussed specific holograms that obey such conditions. The phase modulation $\psi(\phi, a)$ of the CGHs discussed presents odd symmetry in the variable ϕ (the phase of the encoded complex field). Two of the CGHs discussed (identified as CGHs of types 2 and 3) allow reconstruction with a relatively high SNR even if a pixelated SLM is employed for their implementation. This feature is enabled by the highly attenuated amplitudes of high-order diffraction terms of these CGHs that are expressed in terms of integer-order Bessel functions. One of the proposed holograms can be appropriately displayed onto a phase device with a reduced phase range (close to π rad).

We performed numerical simulations on CGHs designed to encode Laguerre–Gauss beams, showing that the pixelated holograms of types 2 and 3 allow signal reconstruction with relatively high SNR. According to the results, the type 3 CGHs present the maximum values of

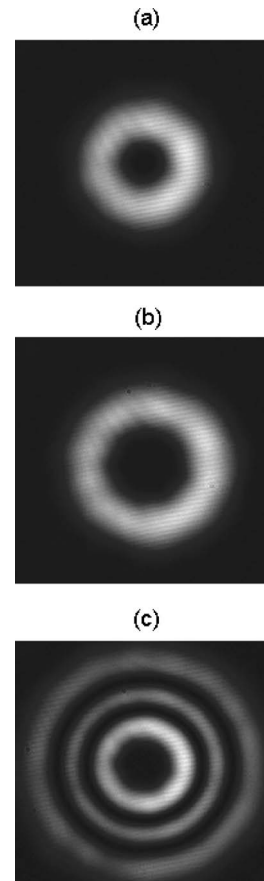


Fig. 10. Experimentally recorded intensity distributions of Laguerre–Gauss beams of indices (a) $(p, l) = (0, 2)$, (b) $(p, l) = (0, 4)$, and (c) $(p, l) = (2, 4)$ generated by type 3 CGHs employing the SLM modulation displayed in Fig. 8.

SNR. However, the type 3 CGHs show smaller efficiency than the type 2 CGHs. Performing additional numerical computations we have proved that CGHs of types 2 and 3 also provide larger SNRs than the point-oriented phase CGHs reported in [6,9–11]. Besides this result, a detailed performance comparison of the novel proposed CGHs with other point-oriented phase CGHs was neglected as beyond the scope of the present paper.

We performed the experimental synthesis of Laguerre–Gauss and nondiffracting Bessel beams of several orders employing a translucent twisted-nematic LC SLM in a phase-mostly configuration that provided a phase range of approximately 1.2π rad. Because of this reduced phase modulation range the complex beams were encoded with type 3 CGHs. The results obtained proved the ability of these CGHs to encode arbitrary complex fields employing a SLM with reduced phase range.

REFERENCES

1. A. W. Lohmann and D. P. Paris, “Binary Fraunhofer holograms generated by computer,” *Appl. Opt.* **6**, 1739–1748 (1967).
2. C. K. Hsueh and A. A. Sawchuk, “Computer-generated double-phase holograms,” *Appl. Opt.* **17**, 3874–3883 (1978).
3. W. J. Dallas, “Computer-generated holograms,” in *The Computer in Optical Research*, B. R. Frieden, ed. (Springer-Verlag, 1980), pp. 4156–4165.

4. N. Mait and K.-H. Brenner, "Dual-phase holograms: improved design," *Appl. Opt.* **26**, 4883–4892 (1987).
5. O. Bryngdahl and F. Wyrowski, "Digital Holography-Computer-Generated Holograms," in *Progress in Optics*, Vol. **XXVIII**, E. Wolf, ed. (North-Holland, 1990), pp. 1–86.
6. R. W. Cohn and M. Liang, "Approximating fully complex spatial modulation with pseudorandom phase-only modulation," *Appl. Opt.* **33**, 4406–4415 (1994).
7. V. Kettunen, P. Vahimaa, J. Turunen, and E. Noponen, "Zeroth-order coding of complex amplitude in two dimensions," *J. Opt. Soc. Am. A* **14**, 808–815 (1997).
8. D. Mendlovic, G. Shabtay, U. Levi, Z. Zalevsky, and E. Marom, "Encoding technique for design of zero-order (on-axis) Fraunhofer computer-generated holograms," *Appl. Opt.* **36**, 8427–8434 (1997).
9. J. A. Davis, D. M. Cottrell, J. Campos, M. J. Yzuel, and I. Moreno, "Encoding amplitude information onto phase-only filters," *Appl. Opt.* **38**, 5004–5013 (1999).
10. M. A. A. Neil, T. Wilson, and R. Juškaitis, "A wavefront generator for complex pupil function synthesis and point spread function engineering," *J. Microsc.* **197**, 219–223 (2000).
11. V. Arrizón, "Optimum on-axis computer-generated hologram encoded into low-resolution phase-modulation devices," *Opt. Lett.* **28**, 2521–2523 (2003).
12. V. Arrizón, G. Méndez, and D. Sánchez-de-La-Llave, "Accurate encoding of arbitrary complex fields with amplitude-only liquid crystal spatial light modulators," *Opt. Express* **13**, 7913–7927 (2005).
13. G. N. Watson, *A Treatise on the Theory of Bessel Functions*, 2nd ed. (Cambridge U. Press, 1922), p. 22.
14. A. Ashkin and J. M. Dziedzic, "Optical trapping and manipulation of single living cells using infrared-laser beams," *Ber. Bunsenges. Phys. Chem.* **93**, 254–260 (1989).
15. A. Ashkin, K. Schutze, J. M. Dziedzic, U. Euteneuer, and M. Schliwa, "Force generation of organelle transport measured *in vivo* by an infrared laser trap," *Nature (London)* **348**, 346–348 (1990).
16. W. H. Wright, G. J. Sonek, Y. Tadir, and M. W. Berns, "Laser trapping in cell biology," *Int. J. Quantum Chem.* **26**, 2148–2157 (1990).
17. I. Moreno, J. Campos, C. Gorecki, and M. J. Yzuel, "Effects of amplitude and phase mismatching errors in the generation of a kinoform for pattern recognition," *Jpn. J. Appl. Phys., Part 1* **34**, 6423–6434 (1995).
18. R. Ponce, A. Serrano-Heredia, and V. Arrizón, "Simplified optimum phase-only configuration for a TNLCD," *Proc. SPIE* **5556**, 206–213 (2004).
19. H. Kim and Y. H. Lee, "Unique measurement of the parameters of a twisted-nematic liquid-crystal display," *Appl. Opt.* **44**, 1642–1649 (2005).